Mode mixing performance evaluation and influence of elements on the fiber system behaviour

Article · March 2023

CITATIONS
0

READS
30

6 authors, including:

Suneela Bhoompallu
Mallareddy Engineering College
15 PUBLICATIONS **6** CITATIONS
SEE PROFILE

Hasane Ahammad Shaik
K L University
146 PUBLICATIONS **609** CITATIONS
SEE PROFILE

Twana Kak Anwer
Salahaddin University - Erbil
33 PUBLICATIONS **11** CITATIONS
SEE PROFILE

Md. Amzad Hossain
Ruhr-Universität Bochum
125 PUBLICATIONS **535** CITATIONS
SEE PROFILE

Shanmugapriya Ganesan, Suneela Bhoompally, Shaik Hasane Ahammad, Kasi Uday Kiran, Twana Mohammed Kak Anwer, Md. Amzad Hossain*, Ahmed Nabih Zaki Rashed* and Walid Fahim Zidan

Mode mixing performance evaluation and influence of elements on the fiber system behaviour

https://doi.org/10.1515/joc-2023-0004
Received January 4, 2023; accepted March 4, 2023;
published online March 23, 2023

Abstract: This study has clarified various micro electro mechanical system (MEMS) processes performance evaluation based on MEMSolver simulation software. The spin time against final resist thickness for the spin coating of a thin film of photo resist and the oxidation time versus oxide thickness for silicone dioxide growth for <100> silicon in wet oxide are clarified. The diffusion profile for Boron after predeposition and drive in of dopants in silicon and the thickness of silicon dioxide mask for Boron diffusion are demonstrated. The dopant distribution resulting from ion implantation and drive in and the percentage of dose penetrating photo resist mask versus thickness of the mask are reported. The film stress versus the film thickness from wafer bow measurements, aluminum deposition rate against temperature using the electronic beam evaporator and the deposition rate of polysilicon versus silane partial pressure are reported. The etch rate of the thermal oxide against percentage concentration of KOH, the etch rate against the etchant temperature for silicon nitride in hot phosphoric acid, and the etch rate against the etchant temperature for the thermal oxide using buffered hydrofluoric acid (BOE) are outlined.

Keywords: diffusion; film deposition and wet etching; implantation; lithography; oxidation.

***Corresponding authors: Md. Amzad Hossain**, Institute of Theoretical Electrical Engineering, Faculty of Electrical Engineering and Information Technology, Ruhr University Bochum, 44801 Bochum, Germany; and Department of Electrical and Electronic Engineering, Jashore University of Science and Technology, 7408 Jashore, Bangladesh,
E-mail: mahossain.eee@gmail.com; and **Ahmed Nabih Zaki Rashed**, Electronics and Electrical Communications Engineering Department, Faculty of Electronic Engineering, Menoufia University, 32951 Menouf, Egypt; and Department of VLSI Microelectronics, Institute of Electronics and Communication Engineering, Saveetha School of Engineering, SIMATS, 602105 Chennai, Tamilnadu, India, E-mail: ahmed_733@yahoo.com.
https://orcid.org/0000-0002-5338-1623
Shanmugapriya Ganesan, Department of ECE, Agnel Institute of Technology and Design, Goa, India, E-mail: spriyagsn@yahoo.com
Suneela Bhoompally, Department of ECE, Malla Reddy Engineering College, 500043 Telagana, India, E-mail: sunilareddyk@gmail.com
Shaik Hasane Ahammad, Department of ECE, Koneru Lakshmaiah Education Foundation, 522302 Vaddeswaram, Andhra Pradesh, India, E-mail: ahammadklu@gmail.com
Kasi Uday Kiran, Department of ECE, Koneru Lakshmaiah Education Foundation, 522502 Guntur, India, E-mail: uk_ece@kluniversity.in
Twana Mohammed Kak Anwer, Department of Physics, College of Education, Salahaddin University-Erbil, 44002 Erbil, Kurdistan Region, Iraq, E-mail: twana.anwar1@su.edu.krd
Walid Fahim Zidan, Electronics and Electrical Communications Engineering Department, Faculty of Electronic Engineering, Menoufia University, 32951 Menouf, Egypt,
E-mail: Walid.Fahim.Zidan9090@gmail.com

1 Introduction

There are many types of processes in MEMS such as lithography, oxidation, diffusion, implantation, film deposition and wet etching [1–9]. The lithography process includes the spin resist where the spin coating of a thin film of photo resist is studied [10–22]. The oxidation process includes the oxidation time in order to estimate the oxidation time to grow the silicon dioxide [23–36]. The diffusion process includes the traditional diffusion which the diffusion profile for the predeposition and drive-in in silicon [37–45]. The diffusion mask is clarified based on the silicon dioxide mask for high temperature diffusion [46–57]. The implementation process includes the traditional implantation which the ion implantation and drive in of main dopants in silicon [58–70]. The implant mask which the mask thickness for selective implantation of dopants are reported mathematically [71–85]. The film Deposition includes the film stress which the thin film stress to be estimated mathematically from wafer bow measurements [86–95]. The evaporation process which the deposition rate of metals using E-beam planetary evaporator is evaluated by using the mathematical relations [96–107]. The wet etching process includes KOH etching, membrane etch, phosphoric acid and buffered HF

[108–120]. The phosphoric acid process which discuss the etch rate of silicon nitride and silicon dioxide in phosphoric acid. The buffered HF which discuss the etch rate of thermal oxide in buffered hydrofluoric acid (BOE) [121–145].

2 Models performance parameters and results discussions

Figure 1 clarifies the spin time against final resist thickness for the spin coating of a thin film of photoresist. The spin time decreases linearly with the final resist thickness varies from 0.1 to 40 μm. Where the initial height of resist is 400 μm, the desired final height of resist is 2 μm, rotational speed of chuck is 20,000 rpm, and kinematic viscosity of resist is 10,000 cSt. The spin coating of a thin film of photo resist is designed through the time of rotation of chuck is 7.122 min.

Figure 2 illustrates the oxidation time versus oxide thickness for silicone dioxide growth for <100> silicon in wet oxide. Where the oxide thickness is 0.5 μm, the oxidation Temperature is 1010 °C and atmosphere is Wet O_2. The oxidation time increases linearly with the oxide thickness varies from 0.01 μm to 10 μm. In order to calculate oxidation time to grow silicon dioxide, the desired oxidation time in Wet oxide O_2 is 79.80 min.

Figure 3 shows the diffusion profile for Boron after predeposition and drive in of dopants in silicon. The Boron concentration decreases exponentially with the depth in silicone varies from 0.001 to 0.17 μm in the predeposition case. The Boron concentration decreases exponentially with the depth in silicone varies from 0.001 to 1.6 μm in the drive in case. The Epi/Substrate wafer type is N-Type, the Epi/Substrate resistivity [ohm-cm] is 1, the dopant type is Boron, the temperature is 940 °C, the time is 20 min, the temperature is 1100 °C, the time is 45 min. The diffusion profile for pre-deposition and drive-in of dopants in silicon is designed. The surface concentration is 7.866E+018 atoms/cm^3, Final junction depth is 1.539 μm and Sheet resistance is 216.44 Ω/sq.

Figure 4 illustrates the thickness of silicon dioxide mask for Boron diffusion. The silicon dioxide mask thickness increases linearly with the diffusion time varies from 10 min to 1000 min. Where the diffusion temperature is 1090 °C, the diffusion time is 87 min and the dopant type is Boron. The silicon dioxide mask for high temperature diffusion is designed. So the thickness of the Silicon dioxide mask is 0.1551 μm.

Figure 5 indicates the dopant distribution resulting from ion implantation and drive in. The Boron concentration increases exponentially with the depth in silicon varies from 0.001 μm to 0.3 μm in the case of implant. But the Boron concentration increases exponentially with the depth in silicon varies from 0.31 μm to 1.4 μm in the case of drive in. Where the Epi/Substrate wafer type is N-Type, the Epi/Substrate resistivity is 1 Ω-cm, the dopant Type is Boron, the implant energy is 80 keV, the Implant dose is 230,000,000,000,000/cm^2, the temperature is 1070 °C, the time is 45 min. The ion implantation and drive-in of dopants in silicon is designed to estimate the peak concentration is 6.505E+018 atoms/cm^3, junction depth after

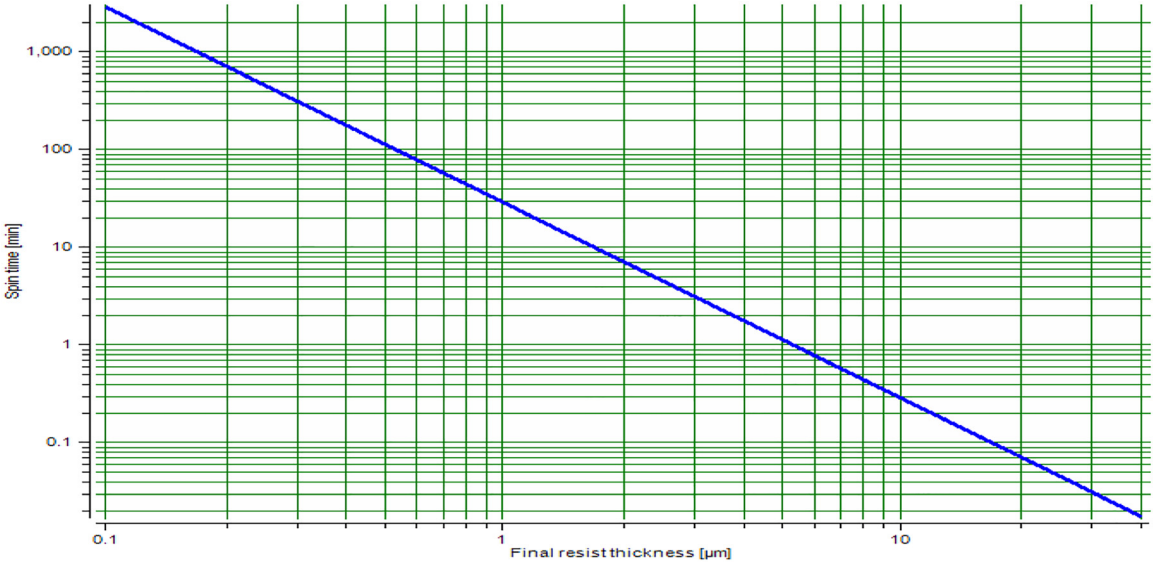

Figure 1: Spin time against final resist thickness.

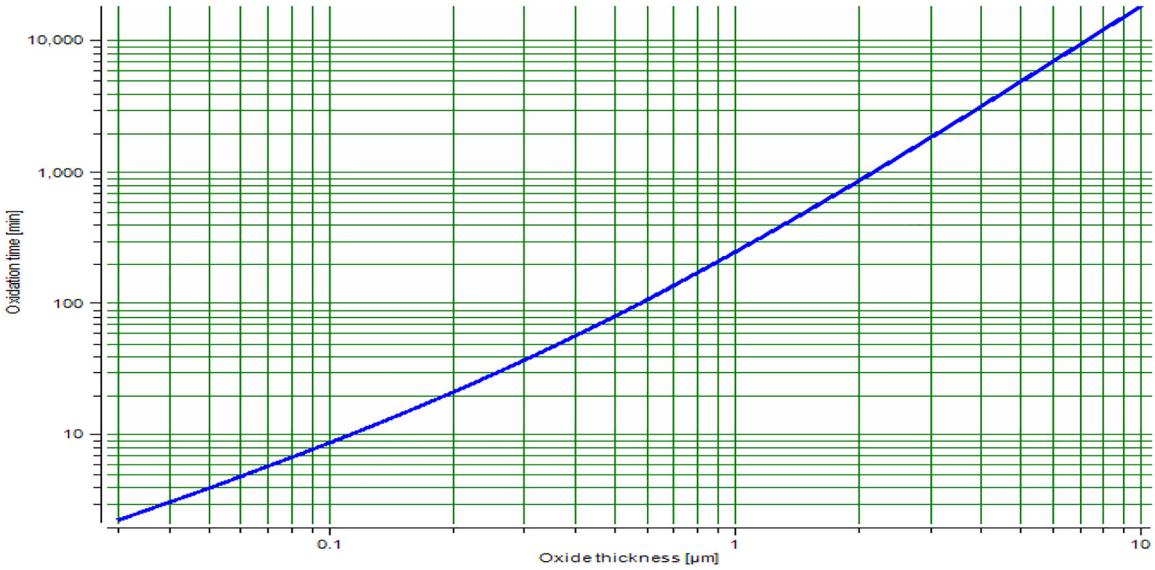

Figure 2: Oxidation time versus oxide thickness for silicone dioxide growth for <100> silicon in wet oxide.

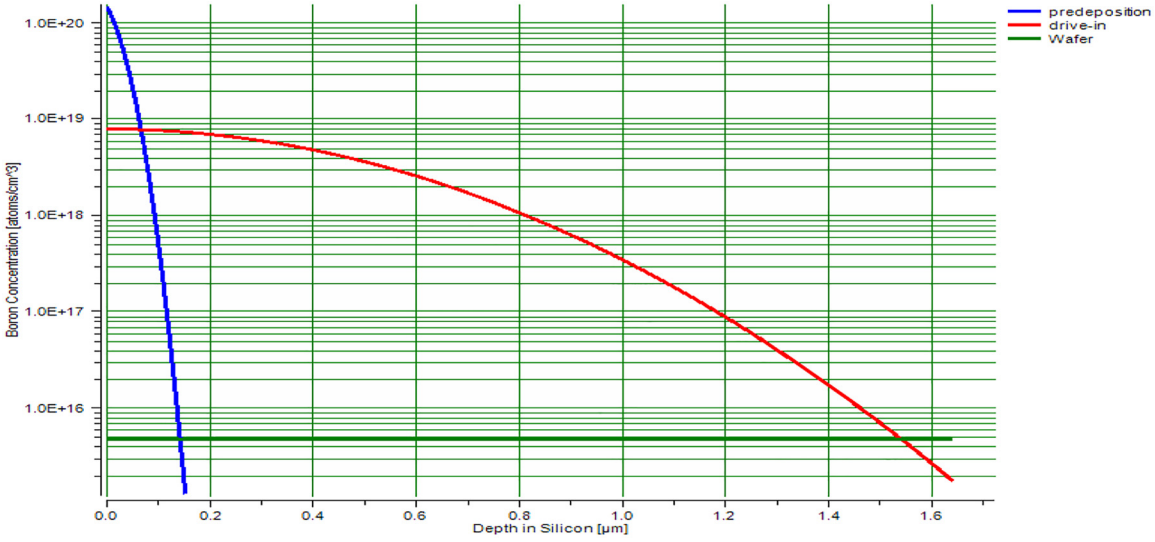

Figure 3: Boron concentration versus depth in silicon in predeposition, drive in cases.

drive-in is 1.412 µm and the sheet resistance after drive-in is 357.85 Ω/sq.

Figure 6 clarifies the percentage of dose penetrating photo resist mask versus thickness of the mask. The mask thickness decreases exponentially with the percentage of dose penetrating photo resist mask varies from 1 to 50%. Where the implant energy is 95 keV, the percentage of dose penetrating mask is 10% and the dopant type is Boron. The mask thickness for selective implantation of dopants is designed to estimate the minimum silicon dioxide mask thickness should be 0.389 µm and the minimum photo resist mask thickness should be 0.7391 µm.

Figure 7 illustrates the film stress versus the film thickness from wafer bow measurements. The film stress decreases linearly with the film thickness varies from 0.01 to 20 µm. Where the bow before deposition is 0.2 µm, the bow after deposition is 6 µm, the thickness of film is 0.2 µm, the thickness of substrate is 400 µm, the diameter of wafer is 100 mm, Young's modulus of substrate is 180 GPa and Poisson's ratio is 0.3. The thin film stress calculated from wafer bow measurements which gives the stress in the film is 159.086 MPa.

Figure 8 shows aluminum deposition rate against temperature using Electronic beam evaporator. Aluminum

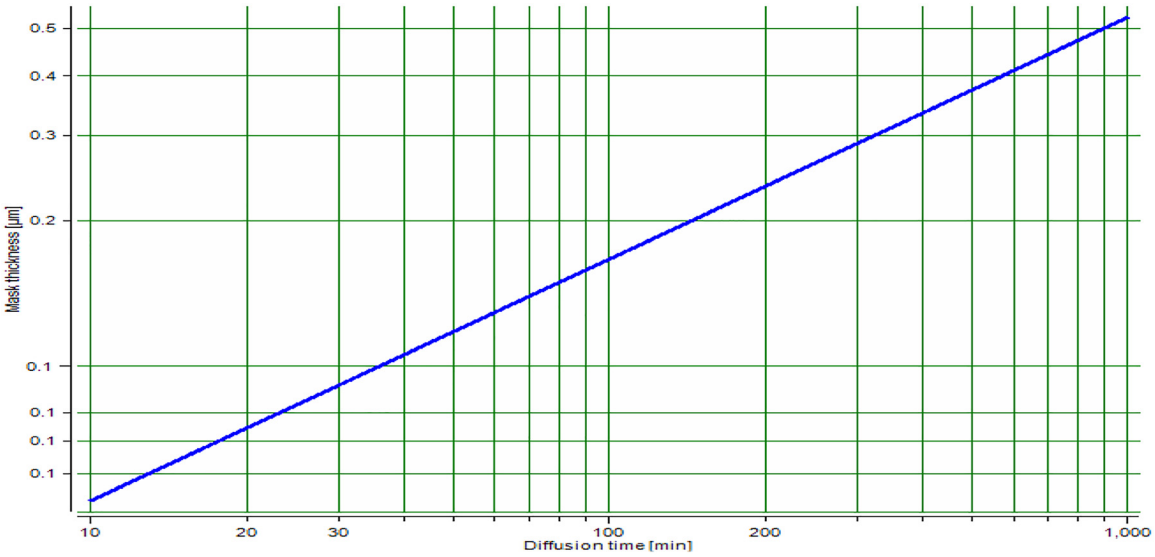

Figure 4: Mask thickness versus the diffusion time for Boron diffusion.

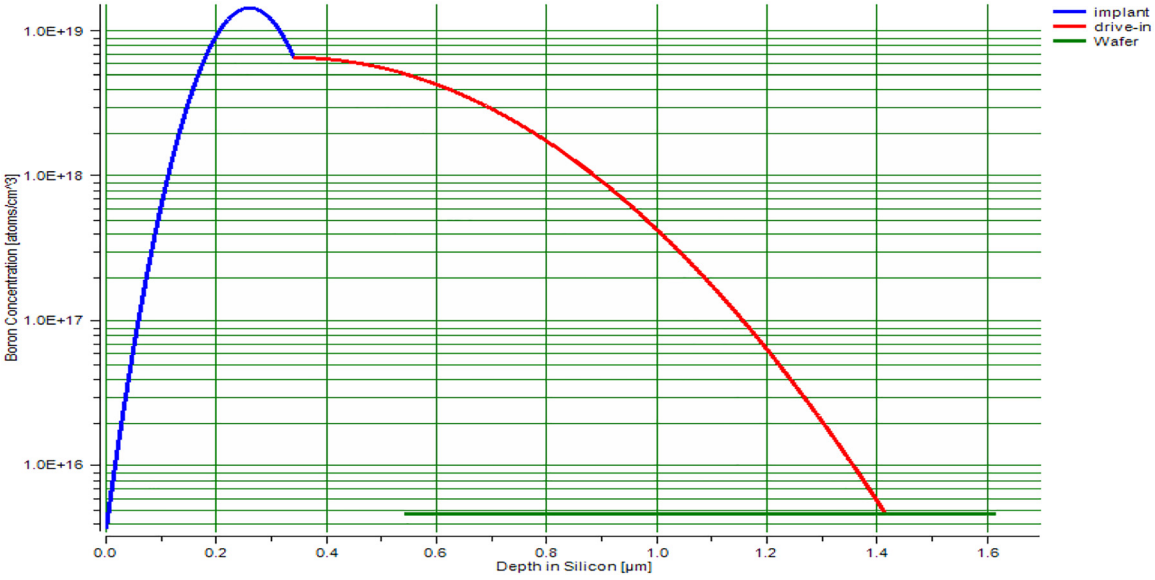

Figure 5: Boron concentration versus the depth in silicon from ion implantation and drive in.

deposition rate increases exponentially with the temperature varies from 900 to 1500 °C. Where the temperature of metal charge is 1150 °C, the radius of the planetary holder is 40 cm, the diameter of the crucible is 5 cm and evaporated metal is aluminum. The deposition rate of metals using E-beam planetary evaporator in order to estimate the deposition rate of Aluminum is 57.761 Å/min.

Figure 9 demonstrates the deposition rate of polysilicon versus silane partial pressure. The deposition rate increases exponentially with the silane partial pressure varies from 1 to 750 mTorr. Where the deposition temperature is 959 °C, the percentage of silane concentration is 30% and the total pressure is 300 mTorr. The deposition rate of polysilicon using silane in a low pressure reactor is designed to give the polysilicon deposition rate is 57.9 Å/min.

Figure 10 illustrates the etch rate of the thermal oxide against percentage concentration of KOH. The etch rate increases linearly with the etchant concentration percentage varies from 10 to 30%, but The etch rate slightly changes as a flat step with the etchant concentration percentage varies from 31 to 35% and the etch rate decreases linearly with the etchant concentration

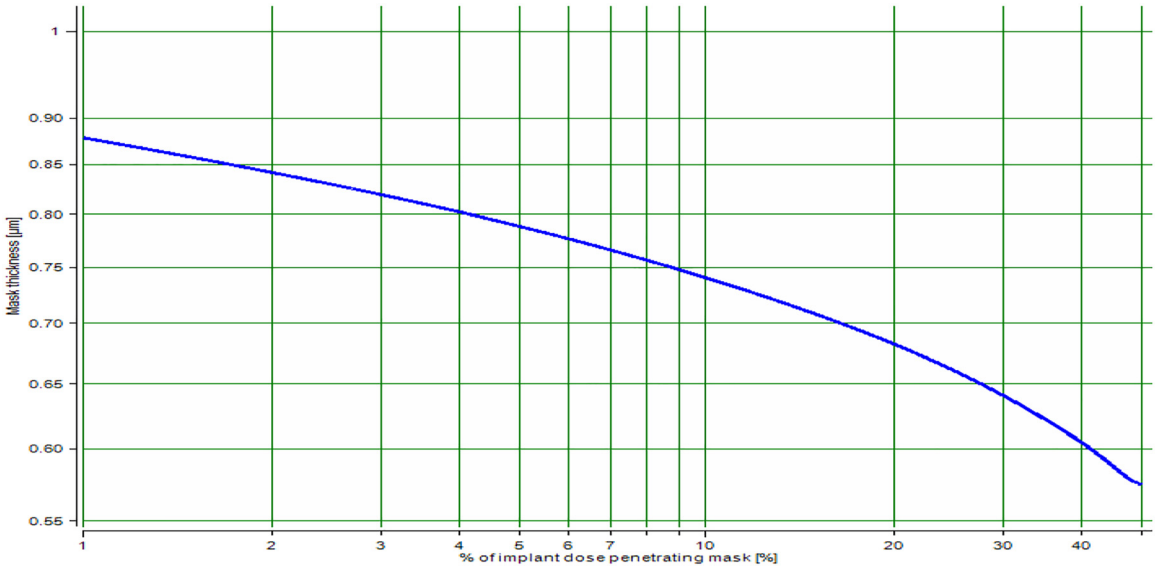

Figure 6: Percentage of dose penetrating photo resist mask versus thickness of the mask.

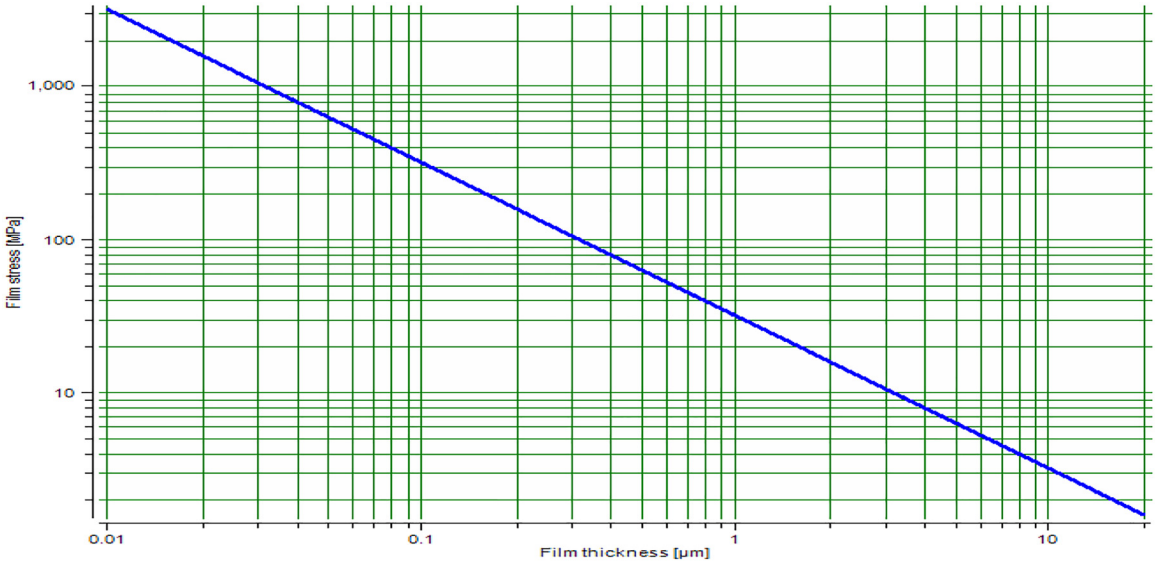

Figure 7: Film stress versus the film thickness from wafer bow measurements.

percentage varies from 36 to 60%. Where the etchant temperature is 30 °C, the etchant concentration is 45 wt% and the etchant is KOH/water. The etch rate of silicon and silicon dioxide in KOH is estimated to clarify the etch rate of <100> silicon in KOH/water etchant is 2.224 µm/h, Etch rate of <110> silicon in KOH/water etchant is 3.331 µm/h and Etch rate of thermal oxide in KOH/water etchant is 3.644 nm/h.

Figure 11 clarifies the mask opening versus the membrane thickness and the size of the mask opening for membrane etch using KOH is simulated. The mask opening decreases linearly with the membrane thickness varies from 2 to 25 µm. Where the thickness of wafer is 400 µm, the thickness of membrane is 15 µm and the size of membrane is 1000 µm. To determine size of mask opening for membrane etch using KOH to give the size of the mask opening is 1545.3 µm.

Figure 12 demonstrates the etch rate against the etchant temperature for silicon nitride in hot phosphoric acid. The etch rate increases with the etchant temperature increases from 145 to 168 °C. Where the etchant temperature is 160 °C, the etchant concentration is 89 wt% and the

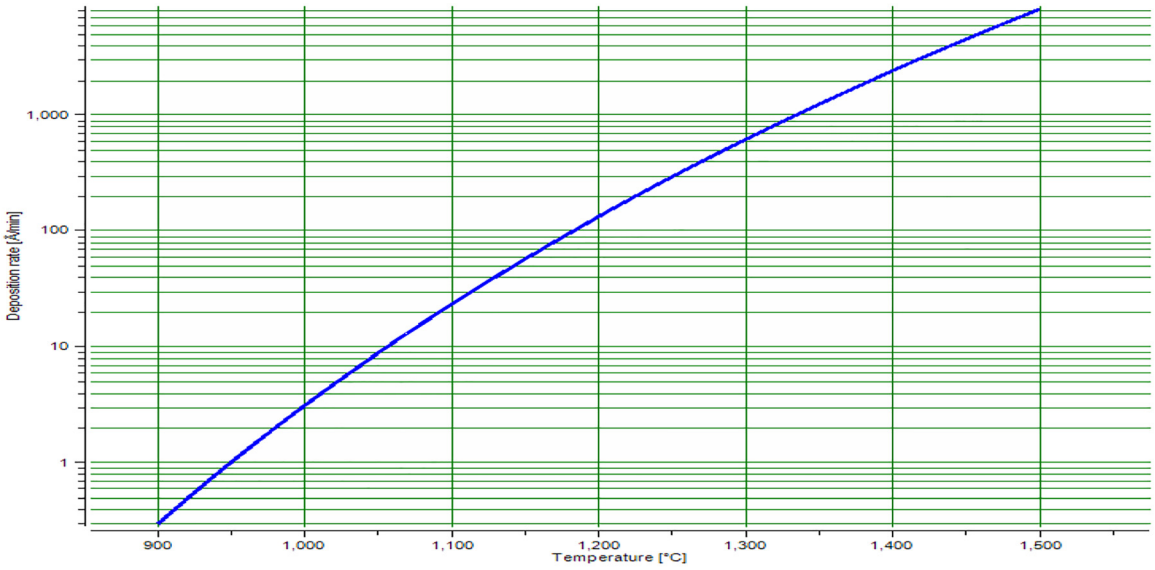

Figure 8: Aluminum deposition rate against temperature using electronic beam evaporator.

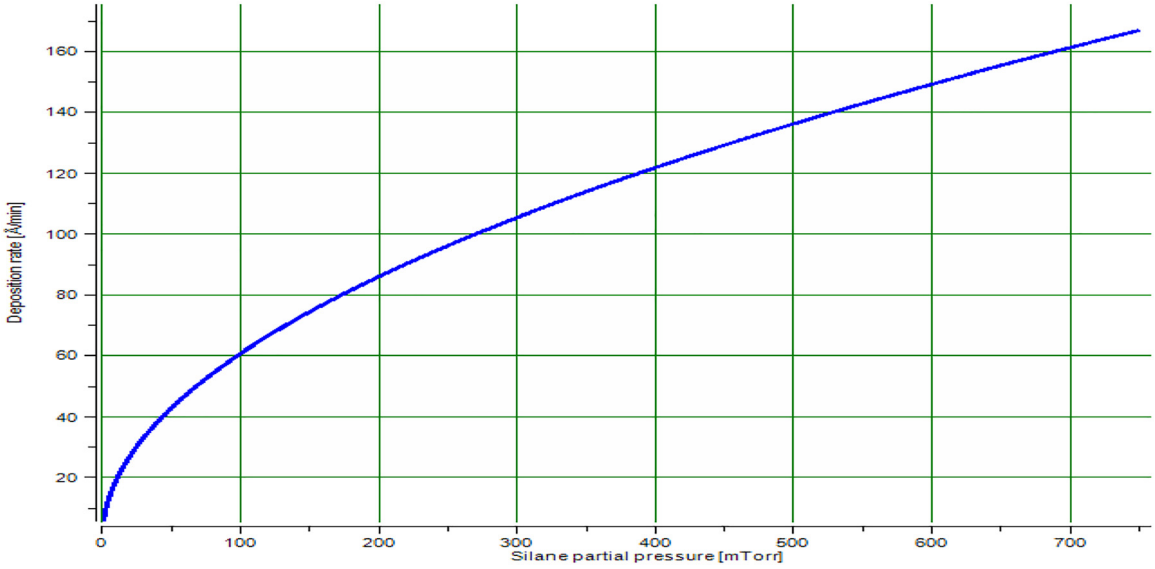

Figure 9: Deposition rate of polysilicon versus silane partial pressure.

film type is the silicon nitride. The etch rate of silicon nitride and silicon dioxide in phosphoric acid is estimated in order to clarify the etch rate at the given temperature is 49.34 Å/min and maximum etch rate at the given concentration is 74.05 Å/min.

Figure 13 shows the etch rate against the etchant temperature for the thermal oxide using BOE. The etch rate increases with the etchant temperature increases from 20 to 40 °C. The etchant temperature is 32 °C, the etchant concentration is 2.4 wt% and the film type is the thermal oxide. The etch rate of thermal oxide in buffered hydrofluoric acid (BOE) is estimated in order to calculate the etch rate of thermal oxide in buffered HF is 600 Å/min.

3 Conclusions

Various MEMS processes performance evaluation based on MEMSolver simulation software have been simulated. The spin coating of a thin film of photo resist is designed through the time of rotation of chuck is 7.122 min. In order to calculate oxidation time to grow silicon dioxide, the

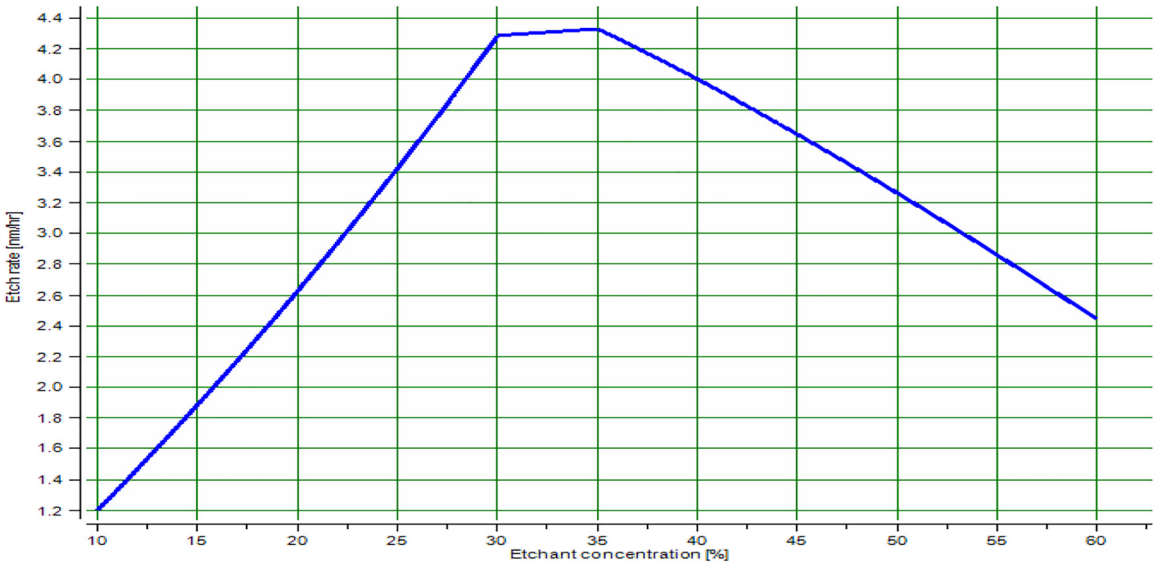

Figure 10: Etch rate against the etchant concentration percentage.

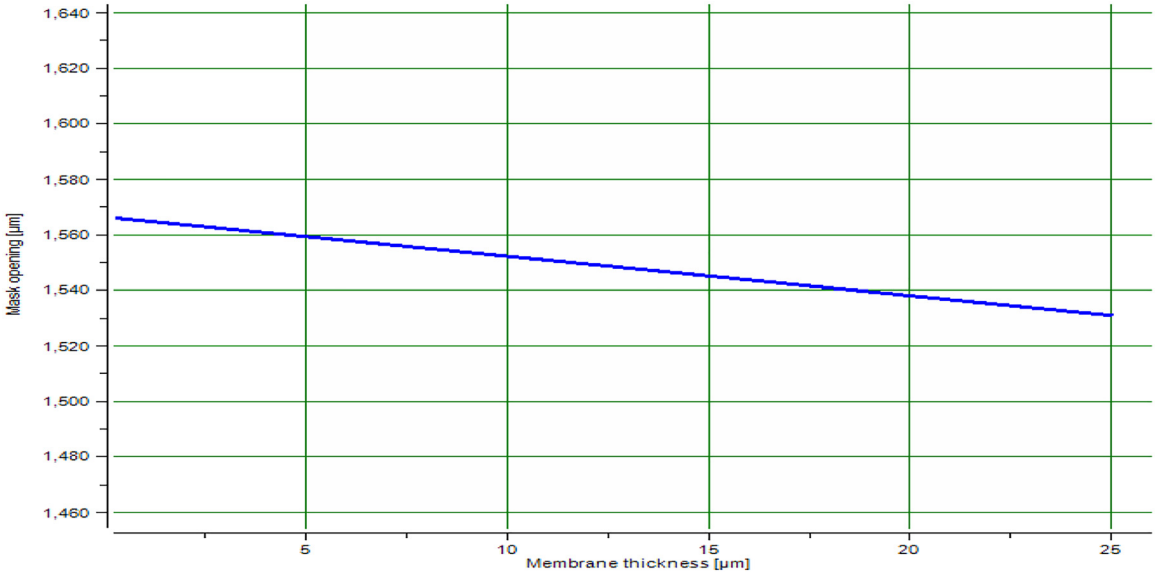

Figure 11: The size of the mask opening for membrane etch using KOH.

desired oxidation time in Wet oxide O_2 is 79.80 min. The diffusion profile for pre-deposition and drive-in of dopants in silicon is designed. The surface concentration is 7.866E+018 atoms/cm^3, Final junction depth is 1.539 µm and Sheet resistance is 216.44 Ω/sq. The silicon dioxide mask for high temperature diffusion is designed. So the thickness of the Silicon dioxide mask is 0.1551 µm. The ion implantation and drive-in of dopants in silicon is designed to estimate the peak concentration is 6.505E+018 atoms/cm^3, junction depth after drive-in is 1.412 µm and the sheet resistance after drive-in is 357.85 Ω/sq. The mask thickness for selective implantation of dopants is designed to estimate the minimum silicon dioxide mask thickness should be 0.389 µm and the minimum photo resist mask thickness should be 0.7391 µm.

The thin film stress calculated from wafer bow measurements which gives the stress in the film is 159.086 MPa. The deposition rate of metals using E-beam planetary evaporator in order to estimate the deposition rate of Aluminum is 57.761 Å/min. The etch rate of silicon and silicon dioxide in KOH is estimated to clarify the etch rate of <100> silicon in KOH/water etchant is 2.224 µm/h, Etch rate of <110>

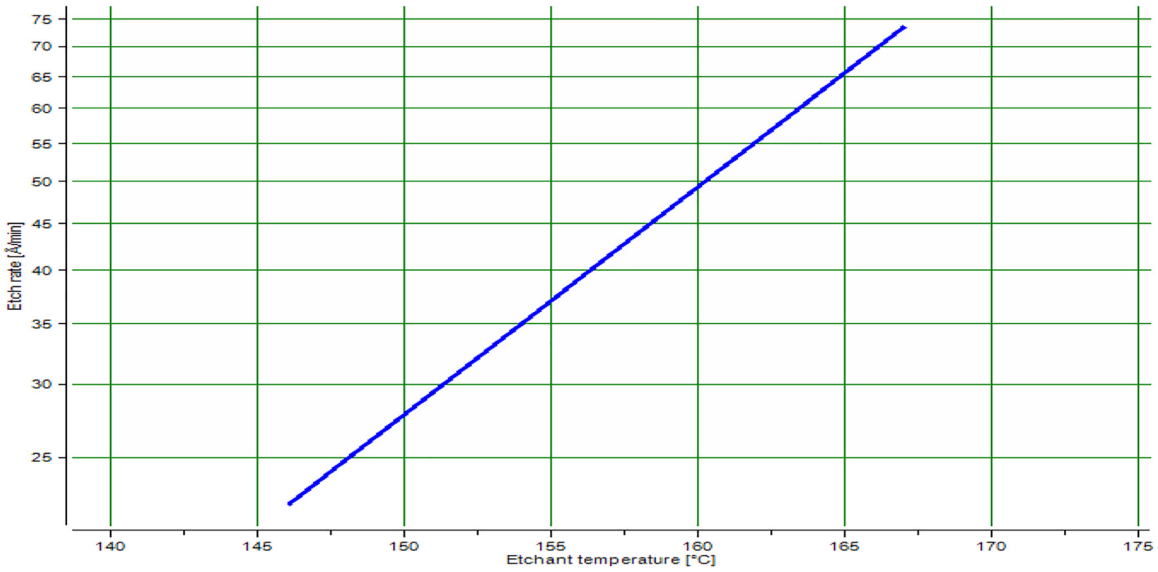

Figure 12: Etch rate against the etchant temperature for silicon nitride in hot phosphoric acid.

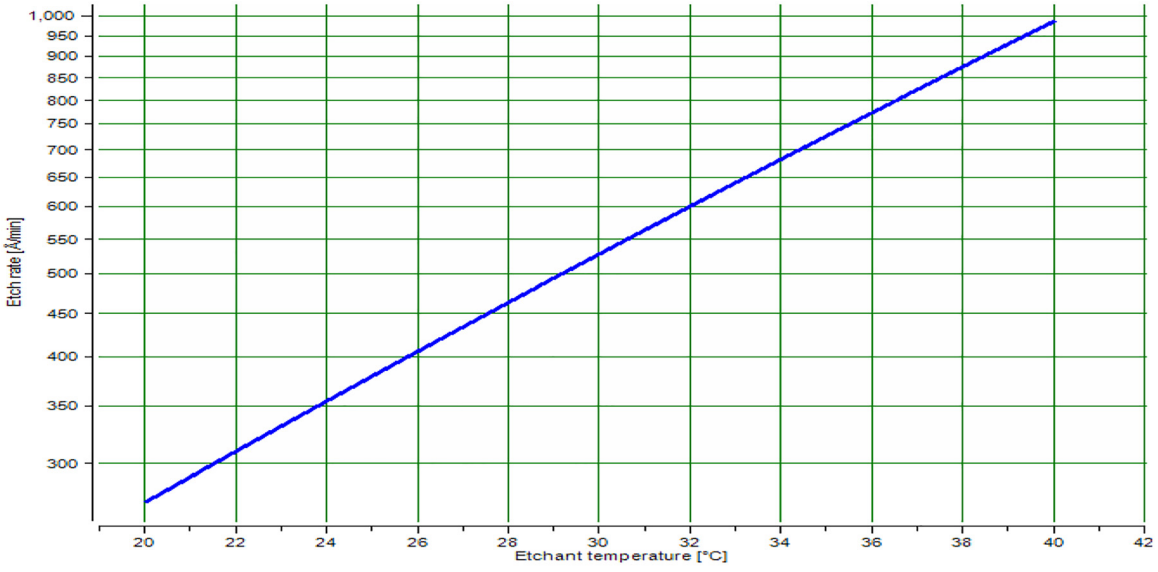

Figure 13: Etch rate against the etchant temperature for the thermal oxide using BOE.

silicon in KOH/water etchant is 3.331 µm/h and Etch rate of thermal oxide in KOH/water etchant is 3.644 nm/h. To determine size of mask opening for membrane etch using KOH to give the size of the mask opening is 1545.3 µm. The etch rate of silicon nitride and silicon dioxide in phosphoric acid is estimated in order to clarify the etch rate at the given temperature is 49.34 Å/min and maximum etch rate at the given concentration is 74.05 Å/min. The etch rate of thermal oxide in buffered hydrofluoric acid (BOE) is estimated in order to calculate the etch rate of thermal oxide in buffered HF is 600 Å/min.

Author contributions: All the authors have accepted responsibility for the entire content of this submitted manuscript and approved submission.
Research funding: None declared.
Conflict of interest statement: The authors declare no conflicts of interest regarding this article.

References

1. Jawad Al-Khaffaf DA. High data rate optical wireless communication system using millimeter wave and optical phase modulation. ARPN J Eng Appl Sci 2018;13:9086–92.
2. Jawad Al-Khaffaf DA, Alshimaysawe IA. Miniaturised tri-band microstrip patch antenna design for radio and millimetre waves of 5G devices. Indones J Electr Eng Comput Sci 2021;21:1594–1601.
3. Al-Khaffaf DAJ, Alsahlany AM. A cloud VLC access point design for 5G and beyond. Opt Quant Electron 2021;53:472–81.
4. Al-Khaffaf DAJ, Alsahlany AM. 60 GHz millimetre wave/10 Gbps transmission for super broadband Wi-Fi network. J Commun 2019;14: 261–6.
5. Al-Khaffaf DAJ, Al-Hamiri MG. Performance evaluation of campus network involving VLAN and broadband multimedia wireless networks using OPNET modeler. TELKOMNIKA 2021;19:1490–7.
6. Alsahlany AM, Al-Khafaf DAJ. An efficient improvement of frame aggregation mechanisms for VHT at MAC and PHY layers in IEEE802. 11ac using MIMO channel. J Theor Appl Inf Technol 2018;96:6817–27.
7. Singh M, Malhotra J, Mani Rajan MS, Dhasarathan V, Aly MH. Performance evaluation of 6.4 Tbps dual polarization quadrature phase shift keying Nyquist-WDM superchannel FSO transmission link: impact of weather conditions. Alex Eng J 2020;59:977–86.
8. Singh M, Malhotra J. A high-speed long-haul wavelength division multiplexing-based inter-satellite optical wireless communication link using spectral-efficient 2-D orthogonal modulation scheme. Int J Commun Syst 2020;33:e4293.
9. Dhasarathan V, Singh M, Malhotra J. Development of high-speed FSO transmission link for the implementation of 5G and Internet of Things. Wireless Network 2019;26:2403–12.
10. Zaki Rashed AN, Tabbour MSF. Best candidate integrated technology for low noise, high speed, and wide bandwidth based transimpedance amplifiers in optical computing systems and optical fiber applications. Int J Commun Syst 2018;31:1–14.
11. Zaki Rashed AN, Tabbour MSF, El-Assar M. 20 Gb/s hybrid CWDM/DWDM for extended reach fiber to the home network applications. Proc Natl Acad Sci India, Sect A Phys Sci 2019;89:653–62.
12. Boopathi CS, Vinoth Kumar K, Sheebarani S, Selvakumar K, Zaki Rashed AN, Yupapin P. Design of human blood sensor using symmetric dual core photonic crystal fiber. Results Phys 2018;11: 964–5.
13. Vigneswaran D, Mani Rajan MS, Aly MH, Zaki Rashed AN. Few-mode ring core fiber characteristics: temperature impact. Photonic Netw Commun J 2019;37:131–8.
14. Praveen Chakkravarthy S, Arthi V, Karthikumar S, Zaki Rashed AN, Yupapin P, Amiri IS. Ultra high transmission capacity based on optical first order soliton propagation systems. Results Phys 2019;12:512–3.
15. Zaki Rashed AN, Vinoth Kumar K, Prithi S, Maheswar R, Tabbour MSF. Transmittivity/reflectivity, bandwidth, and ripple factor level measurement for different refractive index fiber grating shape profiles. J Opt Commun 2019;40:1–15.
16. Zaki Rashed AN, Vinoth Kumar K, Venkatesh Kumar P, Mohamed AE-NA, Tabbour MS, El-Assar M. DWDM channel spacing effects on the signal quality for DWDM/CWDM FTTx network. J Opt Commun 2019;40:30–45.
17. Zaki Rashed AN, Tabbour MSF, Vijayakumari P. Numerical analysis of optical properties using octagonal shaped photonic crystal fiber. J Opt Commun 2019;40:50–65.
18. Zaki Rashed AN, Satheesh Kumar S, Tabbour MSF, Sundararajan TVP, Maheswar R. Different graded refractive index fiber profiles design for the control of losses and dispersion effects. J Opt Commun 2019; 40:75–88.
19. Zaki Rashed AN. Comparison between NRZ/RZ modulation techniques for upgrading long haul optical wireless communication systems. J Opt Commun 2019;40:100–13.
20. Zaki Rashed AN, Vinoth Kumar K, Tabbour MSF, Sundararajan TVP. Nonlinear characteristics of semiconductor optical amplifiers for optical switching control realization of logic gates. J Opt Commun;40: 122–36. https://doi.org/10.1515/joc-2019-0027.
21. Ahmed K, Kumar Paula B, Vasudevan B, Zaki Rashed AN, Maheswar R, Amiri IS, et al. Design of D-shaped elliptical core photonic crystal fiber for blood plasma cell sensing application. Results Phys 2019;12: 2021–5.
22. Ramana TV, Pandian A, Ellammal C, Jarin T, Zaki Rashed AN, Sampathkumar A. Numerical analysis of circularly polarized modes in coreless photonic crystal fiber. Results Phys 2019;13:1–13.
23. Zaki Rashed AN, Mohammed AE-NA, Zaky WF, Amiri IS, Yupapin P. The switching of optoelectronics to full optical computing operations based on nonlinear metamaterials. Results Phys 2019;13:104–15.
24. Ranathive S, Vinoth Kumar K, Zaki Rashed AN, Tabbour MSF, Sundararajan TVP. Performance signature of optical fiber communications dispersion compensation techniques for the control of dispersion management. J Opt Commun 2019;40:148–57.
25. IS Amiri, Zaki Rashed AN, Yupapin P. Interaction between optical sources and optical modulators for high-speed optical communication networks. J Opt Commun 2019;40:176–88.
26. Amiri IS, Zaki Rashed AN, Yupapin P. Effects of order super gaussian pulses on the performance of high data rate optical fiber channel in the presence of self phase modulation. J Opt Commun 2019;40: 200–12.
27. Amiri IS, Zaki Rashed AN, Yupapin P. Mathematical model analysis of dispersion and loss in photonic crystal fibers. J Opt Commun 2019;40: 220–30.
28. Amiri IS, Zaki Rashed AN, Yupapin P. Basic functions of fiber Bragg grating effects on the optical fiber systems performance efficiency. J Opt Commun 2019;40:244–54.
29. Amiri IS, Zaki Rashed AN, Mohammed AE-NA, Aboelazm MB, Yupapin P. Nonlinear effects with semiconductor optical amplifiers. J Opt Commun 2019;40:266–75.
30. Amiri IS, Zaki Rashed AN, Yupapin P. High-speed light sources in high-speed optical passive local area communication networks. J Opt Commun 2019;40:288–300.
31. Zaki Rashed AN, Tabbour MSF, Natarajan K. Performance enhancement of overall LEO/MEO intersatellite optical wireless communication systems. Int J Satell Commun Netw 2020;40:31–40.
32. Amiri IS, Zaki Rashed AN, Mohammed AEA, El-Din ES, Yupapin P. Spatial continuous wave laser and spatiotemporal VCSEL for high-speed long haul optical wireless communication channels. J Opt Commun 2019;40:320–30.
33. Amiri IS, Zaki Rashed AN, Yupapin P. Average power model of optical Raman amplifiers based on frequency spacing and amplifier section stage optimization. J Opt Commun 2019;40:340–55.
34. Amiri IS, Houssien FMA, Zaki Rashed AN, Abd El-Naser AM. Temperature effects on characteristics and performance of near-infrared wide bandwidth for different avalanche photodiodes structures. Results Phys 2019;14:102–10.

35. Amiri IS, Zaki Rashed AN. Simulative study of simple ring resonator-based brewster plate for power system operation stability. Indones J Electr Eng Comput Sci 2019;16:1070–6.
36. Amiri IS, Zaki Rashed AN. Different photonic crystal fibers configurations with the key Solutions for the optimization of data rates transmission. J Opt Commun 2019;40:377–88.
37. Amiri IS, Zaki Rashed AN, Ramya KC, Vinoth Kumar K, Maheswar R. The physical parameters of EDFA and SOA optical amplifiers and bit sequence variations based optical pulse generators impact on the performance of soliton transmission systems. J Opt Commun 2019;40: 400–13.
38. Amiri IS, Houssien FMA, Zaki Rashed AN, Abd El-Naser AM. Optical networks performance optimization based on hybrid configurations of optical fiber amplifiers and optical receivers. J Opt Commun 2019; 40:425–36.
39. Amiri IS, Zaki Rashed AN, Sarker K, Paul BK, Ahmed K. Chirped large mode area photonic crystal modal fibers and its resonance modes based on finite element technique. J Opt Commun 2019;40:455–65.
40. Amiri IS, Houssien FMA, Zaki Rashed AN, Abd El-Naser AM. Comparative simulation of thermal noise effects for photodetectors on performance of long-haul DWDM optical networks. J Opt Commun 2019;40:477–88.
41. Amiri IS, Zaki Rashed AN, Abd El-Naser AM, Aboelazm MB. Single wide band traveling wave semiconductor optical amplifiers for all optical bidirectional wavelength conversion. J Opt Commun 2019;40:503–13.
42. Amiri IS, Zaki Rashed AN, Abd El-Naser AM, Zaky WF. Influence of loading, regeneration and recalling elements processes on the system behavior of all optical data bus line system random access memory. J Opt Commun 2019;40:535–44.
43. Malathy S, Vinoth Kumar K, Zaki Rashed AN, Vigneswaran D, Eeldien ES. Upgrading superior operation performance efficiency of submarine transceiver optical communication systems toward multi tera bit per second. Comput Commun J 2019;146:192–200.
44. Amiri IS, Zaki Rashed AN. Numerical investigation of V shaped three elements resonator for optical closed loop system. Indones J Electr Eng Comput Sci 2019;16:1392–7.
45. Zaki Rashed AN, Tabbour MSF. The engagement of hybrid dispersion compensation schemes performance signature for ultra wide bandwidth and ultra long haul optical transmission systems. Wirel Pers Commun 2019;109:2399–410.
46. Zaki Rashed AN, Tabbour MSF, El-Meadawy S, Anwar T, Sarlan A, Yupapin P, et al. The effect of using different materials on erbium-doped fiber amplifiers for indoor applications. Results Phys;15:103–10. https://doi.org/10.1016/j.rinp.2019.102650.
47. Amiri IS, Zaki Rashed AN. Power enhancement of the U-shape cavity microring resonator through gap and material characterizations. J Opt Commun 2019;40:565–78.
48. Amiri IS, Kuppusamy PG, Zaki Rashed AN, Jayarajan P, Thiyagupriyadharsan MR, Yupapin P. The engagement of hybrid ultra high space division multiplexing with maximum time division multiplexing techniques for high-speed single-mode fiber cable systems. J Opt Commun 2019;40:588–603.
49. Amiri IS, Zaki Rashed AN, Jahan S, Paul BK, Ahmed K. Polar polarization mode and average radical flux intensity measurements based on all optical spatial communication systems. J Opt Commun;40:618–28. https://doi.org/10.1515/joc-2019-0159.
50. Sivaranjani S, Sampathkumar A, Zaki Rashed AN, Sundararajan TVP, Amiri IS. Performance evaluation of bidirectional wavelength division multiple access broadband optical passive elastic networks operation efficiency. J Opt Commun 2019;40:645–60.
51. Amiri IS, Zaki Rashed AN, Yupapin P. High-speed transmission circuits signaling in optical communication systems. J Opt Commun 2019;40: 675–88.
52. Amiri IS, Zaki Rashed AN, Jahan S, Paul BK, Ahmed K, Yupapin P. Technical specifications of the submarine fiber optic channel bandwidth/capacity in optical fiber transmission systems. J Opt Commun 2019;40:701–15.
53. Amiri IS, Zaki Rashed AN. Signal processing criteria based on electro-optic filters for fiber optic access transceiver systems. J Opt Commun 2019;40:733–42.
54. Amiri IS, Zaki Rashed AN, Yupapin P. Pump laser automatic signal control for erbium-doped fiber amplifier gain, noise figure, and output spectral power. J Opt Commun 2019;40:755–70.
55. Amiri IS, Zaki Rashed AN, Parvez AHMS, Bikash Kumar Paul BK, Ahmed K. Performance enhancement of fiber optic and optical wireless communication channels by using forward error correction codes. J Opt Commun 2019;40:786–803.
56. Amiri IS, Zaki Rashed AN, Yupapin P. Z Shaped like resonator with crystal in the presence of flat mirror based standing wave ratio for optical antenna systems. Indones J Electr Eng Comput Sci 2020;17: 1405–9.
57. Amiri IS, Zaki Rashed AN, Yupapin P. Influence of device to device interconnection elements on the system behavior and stability. Indones J Electr Eng Comput Sci 2020;18:843–7.
58. Mahmoud MAE, Amiri IS, Zaki Rashed AN, Yupapin P. Dental lasers applications in visible wavelength operational band. Indones J Electr Eng Comput Sci 2020;18:890–5.
59. Amiri IS, Zaki Rashed AN, Yupapin P. Comparative simulation study of multi stage hybrid all optical fiber amplifiers in optical communications. J Opt Commun 2020;41:12–28.
60. Amiri IS, Zaki Rashed AN, Abdel Kader HM, Al-Awamry AA, et al. Optical communication transmission systems improvement based on chromatic and polarization mode dispersion compensation simulation management. Optik J 2019;207:163–72.
61. Samanta D, Sivaram M, Zaki Rashed AN, Boopathi CS, Amiri IS, Yupapin P. Distributed feedback laser (DFB) for signal power amplitude level improvement in long spectral band. J Opt Commun 2020;41:33–43.
62. Amiri IS, Zaki Rashed AN, Yupapin P. Analytical model analysis of reflection/transmission characteristics of long-period fiber Bragg grating (LPFBG) by using coupled mode theory. J Opt Commun 2020; 41:55–70.
63. Amiri IS, Zaki Rashed AN, Rahman Z, Paul BK, Ahmed K. Conventional/ Phase shift dual drive Mach–Zehnder modulation measured type based radio over fiber systems. J Opt Commun 2020;41:85–100.
64. Alatwi AM, Zaki Rashed AN, El-Eraki AM, Amiri IS. Best candidate routing algorithms integrated with minimum processing time and low blocking probability for modern parallel computing systems. Indones J Electr Eng Comput Sci 2020;19:847–54.
65. El-Hageen HM, Alatwi AM, Zaki Rashed AN. Silicon-Germanium dioxide and aluminum indium gallium arsenide-based acoustic optic modulators. Open Eng J 2020;10:506–11.
66. El-Hageen HM, Alatwi AM, Zaki Rashed AN. RZ line coding scheme with direct laser modulation for upgrading optical transmission systems. Open Eng J 2020;10:546–51.
67. Alatwi AM, Zaki Rashed AN, El-Gammal EM. Wavelength division multiplexing techniques based on multi transceiver in low earth orbit intersatellite systems. J Opt Commun 2020;41:113–22.
68. El-Hageen HM, Kuppusamy PG, Alatwi AM, Sivaram M, Yasar ZA, Zaki Rashed AN. Different modulation schemes for direct and external

modulators based on various laser sources. J Opt Commun 2020;41: 132–40.
69. El-Hageen HM, Alatwi AM, Zaki Rashed AN. High-speed signal processing and wide band optical semiconductor amplifier in the optical communication systems. J Opt Commun 2020;41:155–70.
70. El-Hageen HM, Alatwi AM, Zaki Rashed AN. Laser measured rate equations with various transmission coders for optimum of data transmission error rates. Indones J Electr Eng Comput Sci 2020;20: 1406–12.
71. Eid MMA, Ahasan Habib M, Shamim Anower M, Zaki Rashed AN. Highly sensitive nonlinear photonic crystal fiber based sensor for chemical sensing applications. Microsyst Technol J 2021;27:1007–14.
72. Mahmoud MAE, Zaki Rashed AN, Shafkat A, Ahmed K. Fabry Perot laser properties with high pump lasers for upgrading fiber optic transceiver systems. J Opt Commun 2020;41:188–200.
73. Mahmoud MAE, Zaki Rashed AN, Hosen MS, Paul BK, Ahmed K. Spatial optical transceiver system–based key solution for high data rates in measured index multimode optical fibers for indoor applications. J Opt Commun 2020;41:213–22.
74. Mahmoud MAE, Zaki Rashed AN, El-Meadawy S, Ahmed K. Simulation study of signal gain optimization based on hybrid composition techniques for high speed optically dense multiplexed systems. J Opt Commun 2020;41:235–50.
75. Alatwi AM, Zaki Rashed AN. Hybrid CPFSK/OQPSK modulation transmission techniques' performance efficiency with RZ line coding–based fiber systems in passive optical networks. Indones J Electr Eng Comput Sci 2021;21:263–70.
76. Alatwi AM, Zaki Rashed AN. An analytical method with numerical results to be used in the design of optical slab waveguides for optical communication system applications. Indones J Electr Eng Comput Sci 2021;21:278–86.
77. Alatwi AM, Zaki Rashed AN. Conventional doped silica/fluoride glass fibers for low loss and minimum dispersion effects. Indones J Electr Eng Comput Scii 2021;21:287–95.
78. El-Hageen HM, Alatwi AM, Zaki Rashed AN. Spatial optical transmitter based on on/off keying line coding modulation scheme for optimum performance of telecommunication systems. Indones J Electr Eng Comput Sci 2021;21:305–312.
79. Kurmendra A. High speed optical switching gain based EDFA model with 30 Gb/s NRZ modulation code in optical systems. J Opt Commun 2020;41:288–300.
80. Mahmoud MAE, Zaki Rashed AN, Amiri IS. Fast speed switching response and high modulation signal processing bandwidth through LiNbO3 electro-optic modulators. J Opt Commun 2020;41:312–25.
81. Mahmoud MAE, Mahmoud Houssien FMA, Zaki Rashed AN, Mohammed AE-NA. Performance enhancement of transceiver system based inter satellite optical wireless channel (IS-OWC) for ultra long distances. J Opt Commun 2020;41:345–60.
82. Mahmoud MAE, Zaki Rashed AN, Ehab SED. Simulation performance signature evolution of optical inter satellite links based booster EDFA and receiver preamplifiers. J Opt Commun 2020;41:388–400.
83. Mahmoud MAE, Zaki Rashed AN, Eman ME-G. Influence of dense wavelength division multiplexing (DWDM) technique on the low earth orbit intersatellite systems performance. J Opt Commun 2020;41: 412–26.
84. Mahmoud MAE, Zaki Rashed AN, Al-Mamun Bulbul A, Podder E. Mono rectangular core photonic crystal fiber (MRC-PCF) for skin and blood cancer detection. Plasmonics J 2021;16:717–27.
85. Eid MMA, Seliem AS, Zaki Rashed AN, Mohammed AE-NA, MohamedAli Y, Abaza SS. High speed pulse generators with electro-optic modulators based on different bit sequence for the digital fiber optic communication links. Indones J Electr Eng Comput Sci 2021;21: 957–67.
86. Eid MMA, Seliem AS, Zaki Rashed AN, Mohammed AE-NA, MohamedAli Y, Abaza SS. The key management of direct/external modulation semiconductor laser response systems for relative intensity noise control. Indones J Electr Eng Comput Sci 2021;21: 968–77.
87. Eid MMA, Seliem AS, Zaki Rashed AN, Mohammed AE-NA, MohamedAli Y, Abaza SS. Duobinary modulation/predistortion techniques effects on high bit rate radio over fiber systems. Indones J Electr Eng Comput Sci 2021;21:978–86.
88. Alatwi AM, Zaki Rashed AN. A pulse amplitude modulation scheme based on in-line semiconductor optical amplifiers (SOAs) for optical soliton systems. Indones J Electr Eng Comput Sci 2021;21:1014–21.
89. Mahmoud MAE, Zaki Rashed AN, El-Meadawy S, Habib MA. Best selected optical fibers with wavelength multiplexing techniques for minimum bit error rates. J Opt Commun 2020;21:433–43.
90. Alatwi AM, Zaki Rashed AN, Ismail A, El-Aziz A. High speed modulated wavelength division optical fiber transmission systems performance signature. TELKOMNIKA 2021;19:380–89.
91. Mahmoud MEA, Zaki Rashed AN, El-Gammal EM, Delwar TS, Ryu JY. The influence of electrical filters with sequence generators on optical ISL performance evolution with suitable data rates. J Opt Commun 2020;41:455–70.
92. Alatwi AM, Zaki Rashed AN, Shahriar Parvez AHM, Paul BK, Ahmed K. Beam divergence and operating wavelength bands effects on free space optics communication channels in local access networks. J Opt Commun 2020;41:488–500.
93. Shafkat A, Zaki Rashed AN, El-Hageen HM, Alatwi AM. The effects of adding different adhesive layers with a microstructure fiber sensor based on surface plasmon resonance: a numerical study. Plasmonics J 2021;16:819–32.
94. Mahmoud MEA, Zaki Rashed AN. Fiber optic propagation problems and signal bandwidth measurements under high temperature and high dopant germanium ratios. J Opt Commun 2020;41:512–22.
95. Mahmoud MAE, Zaki Rashed AN. Simulative and analytical methods of bidirectional EDFA amplifiers in optical communication links in the optimum case. J Opt Commun 2020;41:533–50.
96. Mahmoud MAE, Shehata E, Zaki Rashed AN. Cascaded stages of parametric optical fiber amplifiers with Raman fiber amplifiers for upgrading of telecommunication networks through optical wireless communication channel. J Opt Commun 2020;41:566–76.
97. Eid MMA, Mohammed AE-NA, Zaki Rashed AN. Simulative study on the cascaded stages of traveling wave semiconductor optical amplifiers based multiplexing schemes for fiber optic systems improvement. J Opt Commun 2020;41:588–600.
98. Parvin T, Ahmed K, Alatwi AM, Zaki Rashed AN. Differential optical absorption spectroscopy based refractive index sensor for cancer cell detection. Opt Rev 2021;28:134–43.
99. Mahmoud MAE, Mohammed Said S, Zaki Rashed AN. Gain/noise figure spectra of average power model Raman optical amplifiers in coarse wavelength multiplexed systems. J Opt Commun 2020;41: 613–22.
100. Mahmoud MAE, Zaki Rashed AN, Ahammad MS, Paul BK, Ahmed K. The effects of Tx./Rx. pointing errors on the performance efficiency of local area optical wireless communication networks. J Opt Commun 2020;41:633–43.
101. Mahmoud MAE, Huda Said Abd El-Hamid HS, Zaki Rashed AN. High-speed fiber system capacity with bidirectional Er-Yb CDFs based on

differential phase shift keying (DPSK) modulation technique. J Opt Commun 2020;41:654–66.
102. Mahmoud MAE, Ibrahim A, Zaki Rashed AN. In line and post erbium-doped fiber amplifiers with ideal dispersion compensation fiber Bragg grating for upgrading optical access networks. J Opt Commun 2020; 41:688–700.
103. Eid MMA, Ahmed H, Zaki Rashed AN. Chirped Gaussian pulse propagation with various data rates transmission in the presence of group velocity dispersion (GVD). J Opt Commun 2020;42:13–22.
104. Habib A, Zaki Rashed AN, El-Hageen HM, Alatwi AM. Extremely sensitive photonic crystal fiber–based cancer cell detector in the terahertz regime. Plasmonics 2021;16:1297–1306.
105. Shafkat A, Zaki Rashed AN, Hazem M, El-Hageen, Alatwi AM. Design and analysis of a single elliptical channel photonic crystal fiber sensor for potential malaria detection. J Sol Gel Sci Technol 2021;98. 202–211.
106. Eid MMA, Zaki Rashed AN. Fixed scattering section length with variable scattering section dispersion based optical fibers for polarization mode dispersion penalties. Indones J Electr Eng Comput Sci 2021;21:1540–47.
107. Eid MMA, Seliem AS, Zaki Rashed AN, Mohammed AE-NA, MohamedAli Y, Abaza SS. High sensitivity sapphire FBG temperature sensors for the signal processing of data communications technology. Indones J Electr Eng Comput Sci 2021;21:1567–74.
108. Eid MMA, Seliem AS, Zaki Rashed AN, Mohammed AE-NA, MohamedAli Y, Abaza SS. High modulated soliton power propagation interaction with optical fiber and optical wireless communication channels. Indones J Electr Eng Comput Sci 2021;21:1575–83.
109. Mahmoud MAE, Zaki Rashed AN, Delwar TS, Siddique A, Ryu JY. Linear/cubic measured pulse numerically with electrical jitter amplitude variations for the impact on fiber communication systems. J Opt Commun 2021;42:33–43.
110. Eid MMA, El-Meadawy S, Mohammed AE-NA, Zaki Rashed AN. Wavelength division multiplexing developed with optimum length-based EDFA in the presence of dispersion-compensated fiber system. J Opt Commun 2021;42:55–70.
111. Mahmoud MAE, Sorathiya V, Lavadiya S, Habib MA, Ahmed Helmy A, Zaki Rashed AN. Dispersion compensation FBG with optical quadrature phase shift keying (OQPSK) modulation scheme for high system capacity. J Opt Commun 2021;42:86–100.
112. Mahmoud MAE, Sorathiya V, Lavadiya S, Shehata E, Zaki Rashed AN. Free space and wired optics communication systems performance improvement for short-range applications with the signal power optimization. J Opt Commun 2021;42:114–22.
113. Eid MMA, Zaki Rashed AN. Numerical simulation of long-period grating sensors (LPGS) transmission spectrum behavior under strain and temperature effects. Sensor Rev J 2021;41:192–9.
114. Eid MMA, Zaki Rashed AN. Basic FBG apodization functions effects on the filtered optical acoustic signal. Indones J Electr Eng Comput Sci 2021;22:287–96.
115. Mahmoud MAE, El-Meadawy S, Abd El-Naser A. Mohammed AE-NA, Zaki Rashed AN. High data rates in optic fiber systems based on the gain optimization techniques. J Opt Commun 2021;42:130–44.
116. Ahmed K, AlZain MA, Abdullah H, Luo Y, Vigneswaran D, Faragallah OS, et al. Highly sensitive Twin resonance coupling refractive index sensor based on gold- and MgF2-coated nano metal films. Biosensors 2021; 11:104–13.
117. Delwar TS, Siddique A, Ranjan Biswal M, Zaki Rashed AN, Jana Jee A, Ryu Y. Novel multi-user MC-CSK modulation technique in visible light communication. Opt Quant Electron 2021;53:196–206.
118. Eid MMA, Ahasan Habib M, Shamim Anower M, Zaki Rashed AN. Hollow core photonic crystal fiber (PCF)–based optical sensor for blood component detection in terahertz spectrum. Braz J Phys 2021; 51:1017–25.
119. Mahmoud MAE, Sorathiya V, Lavadiya S, Abd El-Hamid HS, Zaki Rashed AN, Wide band fiber systems and long transmission applications based on optimum optical fiber amplifiers lengths. J Opt Commun 2021;42:155–70.
120. Mahmoud MAE, Sorathiya V, Lavadiya S, Shehata E, Zaki Rashed AN. Optical switches based semiconductor optical amplifiers (SOAs) for performance characteristics enhancement by using various electrical pulse generators. J Opt Commun 2021;42:183–95.
121. Mahmoud MAE, Zaki Rashed AN, Sorathiya V, Lavadiya S, Habib MA, Amiri IS. GaAs electro-optic absorption modulators performance evaluation, under high-temperature variations. J Opt Commun 2021; 42:200–13.
122. Abdullaha H, Ahmed K, Alama MS, Zaki Rashed AN, Mitua SA, Al-Zahranid FA, et al. High sensitivity refractive index sensor based on triple layer MgF2-gold-MgF2 coated nano metal films photonic crystal fiber. Optik 2021;241:166–76.
123. Eid MMA, Sorathiya V, Lavadiya S, Abd El-Aziz IA, Zaki Rashed AN. Free space optics communication channel with amplitude/frequency shift keying modulation technique based raised cosine line coding. J Opt Commun 2021;42:225–36.
124. Eid MMA, Zaki Rashed AN, Rajagopal M, Parimanam J, Abhay V. Integrated role between VCSEL diodes and Gaussian pulse generators with ideal EDFA for self phase modulation instability management. J Opt Commun 2021;42:255–70.
125. Mahmoud MAE, Sorathiya V, Lavadiya S, Helmy A, Zaki Rashed AN. Technical specifications and spectral performance characteristics of dispersion flattened fiber (DFF) in optical fiber systems. J Opt Commun 2021;42:280–95.
126. Eid MMA, Zaki Rashed AN. Hybrid NRZ/RZ line coding scheme based hybrid FSO/FO dual channel communication systems. Indones J Electr Eng Comput Sci 2021;22:866–873.
127. Al-Mamun Bulbul A, Zaki Rashed AN, Hazem M, El-Hageen, Alatwi AM. Design and numerical analysis of an extremely sensitive PCF-based sensor for detecting kerosene adulteration in petrol and diesel. Alex Eng J 2021;60:5419–30.
128. Eid MMA, Sorathiya V, Lavadiya S, Ismail A. El-Aziz A, Asaduzzaman S, Rehana H, Mohammed Ibrahim AE-NA, Zaki Rashed AN. ROF systems performance efficiency based on continuous phase frequency shift keying phase modulation scheme. J Opt Commun 2021;42:305–13.
129. Ahasan Habib M, Shamim Anower M, Ahmed AG, Faragallah OS, Eid MMA, Zaki Rashed AN. Efficient way for detection of alcohols using hollow core photonic crystal fiber sensor. Opt Rev 2021;28:383–92.
130. Eid MMA, Sorathiya V, Lavadiya S, Parmar J, Patel SK, Ahmed Ali S, et al. CWDM communication system based inline erbium-doped fiber amplifiers with the linear geometrical polarization model. J Opt Commun 2021;42:320–33.
131. Sorathiya V, Lavadiya S, Ahmed AG, Faragallah OS, El-sayed HS, Mahmoud M, et al. A comparative study of broadband solar absorbers with different gold metasurfaces and MgF2 on tungsten substrates. J Comput Electron 2021;20:1840–50.
132. Lavadiya SP, Sorathiya V, Kanzariya S, Chavda B, Faragallah OS, Eid MMA, Zaki Rashed AN. Design and verification of novel low profile miniaturized pattern and frequency tunable microstrip patch antenna using two PIN diodes. Braz J Phys 2021;51:1303–13.
133. Eid MMA, Urooj S, Alwadai NM, Zaki Rashed AN. AlGaInP optical source integrated with fiber links and silicon avalanche photo

detectors in fiber optic systems. Indones J Electr Eng Comput Sci 2021; 23:847–54.
134. Zaki Rashed AN, Hasane Ahammad SK, Daher MG, Zyoud SH, Sorathiya V, Montalbo FJP, et al. Various transmission codes for the control of bit error rate in both optical wired and wireless communication channels. J Opt Commun 2022;43:155–66.
135. Asaduzzaman S, Rehana H, Bhuiyan T, Sarma D, Faragallah OS, Mahmoud M, et al. Extremely high birefringent slotted core umbrella-shaped photonic crystal fiber in terahertz regime. Appl Phys B 2022; 128:899–914.
136. Sorathiya V, Lavadiya S, Parmar B, Baxi S, Taher Dhankot, Faragallah OS, et al. Tunable frequency selective surface using crossed shaped graphene metasurface geometry for far infrared frequency spectrum. Appl Phys B 2022;128:1245–65.
137. Zuhayer A, Abd-Elnaby MSHA, Mahmoud M, Eid A, Sorathiya V, Zaki Rashed AN. A gold plated twin core D-formed photonic crystal fiber (PCF) for ultrahigh sensitive applications based on surface plasmon resonance (SPR) approach. Plasmonics J 2022;17:2089–101.
138. Daher MG, Jaroszewicz Z, Zyoud SH, Panda A, Ahammad SKH, Abd-Elnaby M, et al. Design of a novel detector based on photonic crystal nanostructure for ultra high performance detection of cells with diabetes. Opt Quant Electron 2022;54:777–89.
139. Smirani LK, Ahammad SKH, Amzad Hossain M, Daher MG, Fahmy E. Conventional/linear/Lorentzian material gain semiconductor optical amplifiers performance signature with four wave mixing (FWM) nonlinearity in optical fiber communication systems. J Opt Commun 2022;43:202–18.
140. Smirani LK, Kumari M, Ahammad SKH, Hossain MA, Daher MG, Zaki Rashed AN, Anas Ibrahim A, Abohassan KM, Panda A. Signal quality enhancement in multiplexed communication systems based on the simulation model of the optimum technical specifications of Raman fiber optical amplifiers. J Opt Commun 2022; 43:233–45.
141. Smirani LK, Ahammad SKH, Daher MG, Amzad Hossain MA, Zaki Rashed AN, Aabdelhamid HS. Optical transceiver communication systems performance evaluation based on nonlinear cross gain modulation effects. J Opt Commun 2022;43:260–76.
142. Smirani LK, Abd El-Aziz IA, Hossain MA, Daher MG, Zaki Rashed AN. Low loss flexibility and high efficiency of radio per fiber system for modern wireless communication system. J Opt Commun 2022;43: 300–17.
143. Sbeah ZA, Adhikari R, Sorathiya V, Chauhan D, Zaki Rashed AN, Chang SH, Prakash Dwivedi R. GST-based plasmonic biosensor for hemoglobin and urine detection. Plasmonics J 2022;17:2391–404.
144. Daher MG, Trabelsi Y, Ahmed NM, Kumar Prajapati Y, Sorathiya V, Ahammad SH, Poorna Priya P, Faragallah OS, Zaki Rashed AN. Detection of basal cancer cells using photodetector based on a novel surface plasmon resonance nanostructure employing perovskite layer with an ultra high sensitivity. Plasmonics J 2022;17:2365–73.
145. Daher MG, Trabelsi Y, Panda A, Gevorgyan AH, Abohassan KM, Smirani LK, Altahan BR, Zaki Rashed AN. Design of a highly sensitive detector using a ternary photonic crystal (PC) based on titanium nitride sandwiched between Si and SiO_2 for the creatinine concentration detection in the blood serum. Opt J 2022;3:447–61.